JOURNAL OF APPLIED ELECTROCHEMISTRY **27** (1997) 1362–1368

Surface activation of manganese oxide electrode for oxygen evolution from seawater

K. IZUMIYA, E. AKIYAMA, H. HABAZAKI, A. KAWASHIMA, K. ASAMI, K. HASHIMOTO

Institute for Materials Research, Tohoku University, Sendai 980-77, Japan

N. KUMAGAI

Daiki Engineering Company, Ltd, 11 Shintoyofuta, Kashiwa, Chiba 277, Japan

Received 19 February 1996; revised 6 March 1997

Utilizing the fact that the equilibrium potential of oxygen evolution is lower than that of chlorine evolution, oxygen evolution in seawater electrolysis was enhanced by decreasing the polarization potential under galvanostatic conditions through increasing the effective surface area of manganese oxide electrodes. Electrodes were prepared by a thermal decomposition method. IrO_2-coated titanium (IrO_2/Ti electrode) was used as the substrate on which manganese oxide was coated (MnO_X/IrO_2/Ti electrode). Subsequently, oxide mixtures of manganese and zinc were coated (MnO_X–ZnO/MnO_X/IrO_2/Ti electrode). The effective surface area of the MnO_X–ZnO/MnO_X/IrO_2/Ti electrodes was increased by selective dissolution of zinc (leaching) into hot 6 M KOH. The oxygen evolution efficiency of the MnO_X/IrO_2/Ti electrode was 68–70%. Leaching of zinc from the MnO_X–ZnO/MnO_X/IrO_2/Ti electrodes with 25 mol % or less zinc led to a significant increase in the oxygen evolution efficiency. The maximum efficiency attained was 86% after leaching of zinc from the MnO_X–25 mol %ZnO/MnO_X/IrO_2/Ti electrode. However, large amounts of zinc addition, such as 40 mol % or more are detrimental because of a decrease in the oxygen evolution efficiency. This is due to the formation of a double oxide, $ZnMnO_3$, which is hardly dissolved in hot 6 M KOH.

Keywords: *manganese oxide electrode*, *oxygen evolution*, *seawater electrolysis*, *surface activation*

1. Introduction

To avoid global warming, we are studying 'global CO_2 recycling' [1–5]. In this system electricity is generated by solar cells in deserts and transmitted to the nearest coastal area, where the electricity is used for production of hydrogen by electrolysis of seawater. Carbon dioxide is recovered and liquefied at fuel burning plants and transported by tankers to the coasts close to the deserts. Carbon dioxide is converted into methane by reaction with hydrogen produced by seawater electrolysis. Methane is liquefied and transported by tankers to energy consumers.

The most difficult problem concerns the anode for seawater electrolysis. When conventional anode materials are used, both oxygen and chlorine are evolved. However, the anodic reaction must avoid chlorine evolution, that is, anode materials must have high activity and long durability for oxygen evolution without chlorine evolution.

A number of anodes have been used for electrolysis of aqueous solutions. Electrolysis of concentrated NaCl aqueous solution employs noble metal oxide-coated electrodes for chlorine evolution. However, only a few studies of oxygen electrodes for seawater electrolysis have been reported [6, 7]. The equilibrium potential of oxygen evolution in seawater at pH about 8 is 0.745 V [8] which is about 0.6 V lower than that of chlorine evolution. Because of a high overpotential for oxygen evolution, the anode potential of conventional electrodes for seawater electrolysis exceeds the chlorine evolution potential. Among various substances, manganese oxide is known to have a lower overpotential for oxygen evolution than for chlorine evolution [6, 7].

This work is aimed at investigating electrode materials with high oxygen evolution efficiency for seawater electrolysis. Particular attention is paid to the relationship between the electrolytic characteristics and the morphology of the electrode surface.

Electrodes were prepared by thermal decomposition. Because of the lower equilibrium potential of oxygen evolution compared to chlorine evolution, reduction of polarization potential in seawater electrolysis for enhancement of oxygen evolution was attempted by increasing the effective surface area. Surface roughening was performed by leaching of zinc into a hot alkali solution from an electrode surface consisting of an oxide mixture of manganese and zinc.

0021-891X

2. Experimental details

2.1. *Preparation of electrodes*

Substrates used in this work were titanium sheets 25 mm × 70 mm × 1 mm which were previously immersed in 3 wt % HF solution for 3–5 s, rinsed with deionized water and dried in air. These titanium sheets were immersed in hot 80 wt % H_2SO_4 for 10 min, rinsed with deionized water and dried. After this treatment, IrO_2 was coated onto the titanium substrate as an intermediate layer, because the presence of the intermediate IrO_2 layer can prevent formation of insulating titanium oxide between electrocatalytically active manganese oxide and the titanium substrate during electrolysis. The IrO_2 layer was coated as follows: 0.1 M chloroiridic acid butanol solution was coated on the titanium substrate, and the specimen was dried at 80 °C for 10 min and baked at 450 °C for 10 min. This procedure was repeated three times so as to form the coating in which the total iridium was about 10 g m^{-2}. This specimen was finally baked at 450 °C for 1 h [9]. Electrodes so formed are called IrO_2/Ti electrodes. Manganese oxide was coated on the IrO_2/Ti electrode as follows: 0.2 M manganese(II) nitrate butanol solution was coated onto the IrO_2/Ti electrode and the specimen was dried at 80 °C for 10 min and baked at 450 °C for 10 min [10]. This procedure was repeated 30 times, because IrO_2, which has a very high activity for chlorine evolution, must be coated completely by manganese oxide. The total of manganese was about 8×10^{-2} mol m^{-2}. This specimen was finally baked at 450 °C for 1 h. The electrode thus prepared is called the MnO_X/IrO_2/Ti electrode. The manganese oxide coating was also carried out directly on the titanium substrate for comparison (MnO_X/Ti electrode).

Oxide mixtures of manganese and zinc were coated as follows: manganese nitrate and zinc nitrate were dissolved in butanol solution. Concentrations of zinc nitrate were 1, 5, 10, 20, 25, 30, 40 and 50 mol % zinc of the total of zinc and manganese.

These solutions were coated on the manganese oxide layer by the same procedure as that for manganese oxide coating. These electrodes are called the MnO_X–ZnO/MnO_X/IrO_2/Ti electrodes. The nominal compositions of oxide mixtures prepared on the electrodes are expressed as the mol % of zinc mentioned above. These oxides were identified by X-ray diffraction with CuK_α radiation. Specimens 15 mm × 20 mm and 10 mm × 10 mm in area were cut for measurements of oxygen evolution efficiency and potentiodynamic polarization curves, respectively. Surface activation was performed in order to increase the effective surface area by leaching of zinc from the MnO_X–ZnO/MnO_X/IrO_2/Ti electrodes into 6 M KOH aqueous solution at 80 °C for different periods (1, 10, 60 and 360 min) [11]. The specimens were then rinsed with deionized water and dried in air. After a titanium wire was spot-welded to an edge of the specimen, the edges and the back side of the specimens were masked off from the electrode surface using a commercial nail enamel.

2.2. *Electrochemical measurements*

A single compartment type electrochemical cell made of glass was used under a stirring condition. A platinum gauze was used as a counter electrode for potentiodynamic measurements but a platinum wire was used for the measurement of chlorine evolution efficiency in order to avoid reduction of hypochlorite ions on the counter electrode with a large surface area. A saturated calomel electrode (SCE) was used as reference. The electrolyte used was 300 ml of 0.5 M NaCl aqueous solution at 30 °C where pH was adjusted to 8.3 by adding 0.01 M NaOH. Due to chlorine evolution during electrolysis of 0.5 M NaCl solution, the pH increased to about 8.7 after electrolysis. Accordingly, the solution pH is described as 8.3–8.7 in this paper.

The electrode performance for gas evolution was potentiodynamically examined with a potential sweep rate of 50 mV min^{-1}. Correction for ohmic drop was made by using a Hokuto IR compensation instrument.

The oxygen evolution efficiency was measured as follows. To determine the current efficiency for chlorine evolution electrolysis was conducted at 200 A m^{-2} and 30 °C in the 0.5 M NaCl aqueous solution at 100 cm of the ratio of the solution volume to the specimen surface area until 300 C of charge was passed. Because the anode and cathode compartments were not separated from each other, most of the chlorine formed on the anode seemed to be converted to sodium hypochlorite by reaction with sodium hydroxide formed on the cathode. Both chlorine and sodium hypochlorite liberate iodine from potassium iodide. Accordingly, after the electrolysis 5 ml of acetic acid and excess potassium iodide were added to the electrolyte, and the amount of chlorine produced was estimated by titration with an N/100 $Na_2S_2O_3$ solution [12]. The oxygen evolution efficiency was determined by subtraction of the chlorine evolution efficiency from 100%.

2.3. *X-ray photoelectron spectroscopic analysis*

X-ray photoelectron spectroscopy (XPS) by means of Shimadzu ESCA850 electron spectrometer with MgK_α($h\nu = 1253.6$ eV) excitation was employed for the analysis of the specimen surface before and after surface activation in 6 M KOH solution. The binding energies of electrons were calibrated using the method described elsewhere [13, 14]; the binding energies of the Au $4f_{7/2}$ and $4f_{5/2}$ electrons of gold and the Cu $2p_{3/2}$ electrons of copper were taken as 84.07, 87.74 and 932.53 eV, respectively, and the kinetic energy of the Cu $L_3M_{4.5}M_{4.5}$ Auger electrons of copper as 918.65 eV. The composition of the specimen surface was quantitatively determined by the previously proposed method [15, 16], using integrated intensities

of corresponding XPS spectral peaks after subtraction of background. The photoionization cross sections of Mn $2p_{3/2}$ and Zn $2p_{3/2}$ electrons relative to that of the O 1s electrons used were 3.15 and 6.32, respectively [17].

3. Results and discussion

Figure 1 shows X-ray diffraction patterns of as-prepared specimens. The manganese oxide coating without zinc consists of α-Mn_2O_3. An oxide mixture of 25 mol % zinc and 75 mol % manganese is composed of α-Mn_2O_3 and a spinel double oxide $ZnMn_2O_4$. A dark-grey coloured deposit of equal per cent mixture of zinc and manganese is assigned to $ZnMnO_3$. Increasing zinc content results in grain refining of oxide crystals as can be seen from the broadening of the diffraction patterns.

Figure 2 shows potentiodynamic anodic polarization curves of IrO_2/Ti and MnO_X/IrO_2/Ti electrodes measured in 0.5 M NaCl aqueous solution of pH 8.3–8.7 at 30 °C. The potentiodynamic anodic polarization curve of the MnO_X/Ti electrode is also shown for comparison. The MnO_X/Ti electrode without IrO_2 coating as an intermediate layer shows very low current density. According to Morita *et al.* [18], a solid solution of MnO_X coating and titanium substrate is hardly formed at the interface, and therefore a TiO_2 layer with high electric resistivity is formed at the interface between the MnO_X coating and the titanium substrate. The MnO_X/IrO_2/Ti electrode with the intermediate IrO_2 layer shows relatively higher current density than that of the MnO_X/Ti electrode.

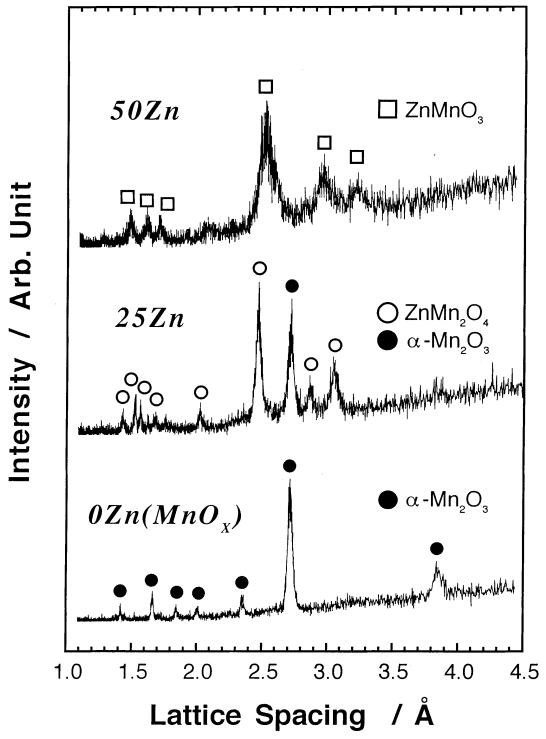

Fig. 1. X-ray diffraction patterns of as-prepared electrodes coated with manganese oxide (0Zn) and manganese-zinc oxides containing 25 (25Zn) and 50 mol % zinc (50Zn).

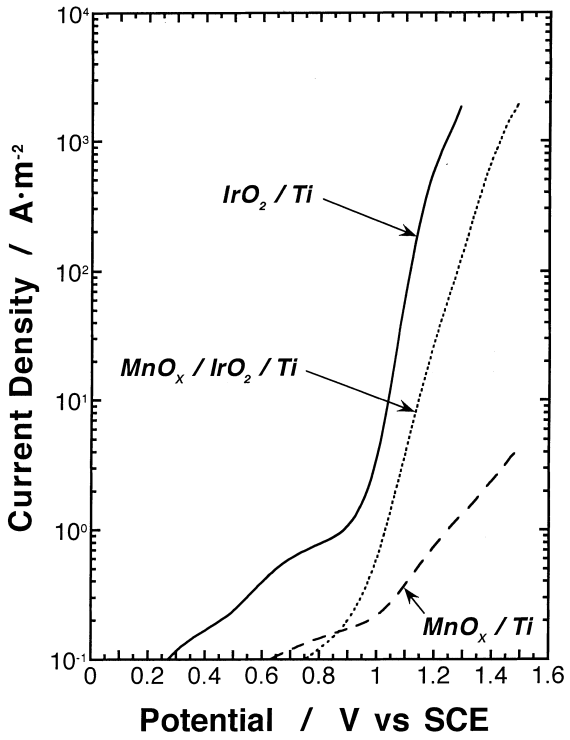

Fig. 2. Potentiodynamic anodic polarization curves of MnO_X/Ti, IrO_2/Ti and MnO_X/IrO_2/Ti electrodes measured in 0.5 M NaCl at 30 °C and pH 8.3–8.7 (Potential IR (ohmic) drop free).

The IrO_2/Ti electrode shows very high current density. As will be shown later, the oxygen evolution efficiency of the MnO_X/IrO_2/Ti electrode is 68–70%, while that of the IrO_2/Ti electrode is only 20% because of the high activity of the IrO_2/Ti electrode for chlorine evolution.

Instead of coating of the oxide mixture on the MnO_X/IrO_2/Ti electrode, direct coating of the oxide mixture on the IrO_2/Ti electrode tends to result in exposure of IrO_2 to 0.5 M NaCl solution after leaching of zinc, and hence the oxygen evolution efficiency of the MnO_X–ZnO/IrO_2/Ti electrode after leaching was only 30–50%. In order to avoid gas evolution on the IrO_2 surface the oxide mixture of manganese and zinc was coated on the MnO_X/IrO_2/Ti electrode.

Figure 3 shows potentiodynamic anodic polarization curves of the MnO_X–ZnO/MnO_X/IrO_2/Ti electrodes before leaching of zinc. The addition of zinc decreases the anodic current and, hence, the formation of double oxides of zinc and manganese decreases the activity for gas evolution. Figure 4 shows the oxygen evolution efficiency of these electrodes before leaching of zinc as a function of the nominal content of zinc. The oxygen evolution efficiency of the MnO_X/IrO_2/Ti electrode is significantly higher than that of the IrO_2/Ti electrode and decreases with zinc addition. Accordingly, the zinc addition is detrimental for oxygen evolution and surface activation by zinc leaching is necessary.

Figure 5 shows potentiodynamic anodic polarization curves of the MnO_X–25 mol % ZnO/MnO_X/

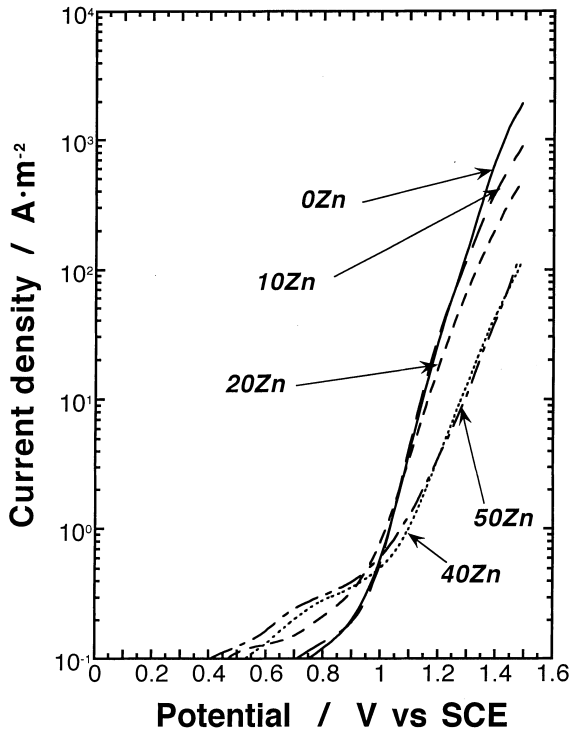

Fig. 3. Potentiodynamic anodic polarization curves of as-prepared MnO_X–ZnO/MnO_X/IrO_2/Ti electrodes measured in 0.5 M NaCl at 30 °C and pH 8.3–8.7 (Potential IR (ohmic) drop free).

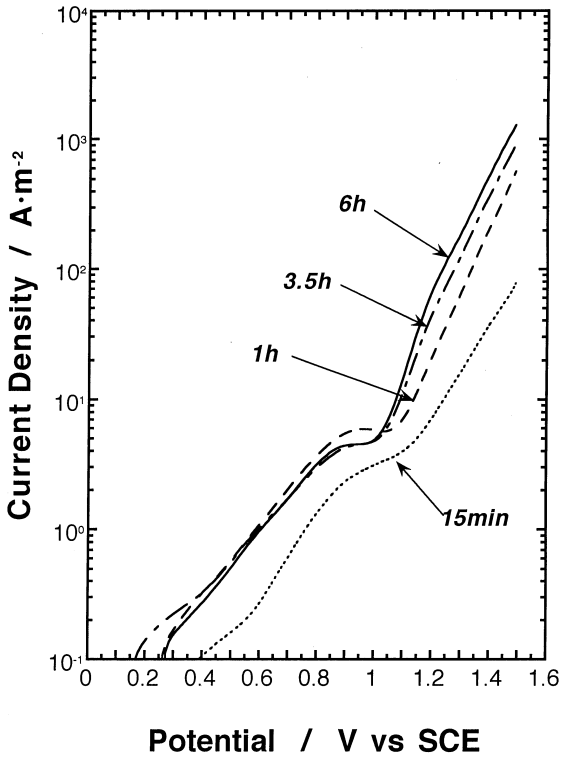

Fig. 5. Potentiodynamic anodic polarization curves of MnO_X–25 mol % ZnO/MnO_X/IrO_2/Ti electrodes surface-activated for 15 min, 1 h, 3.5 h and 6 h measured in 0.5 M NaCl at 30 °C and pH 8.3–8.7 (Potential IR (ohmic) drop free).

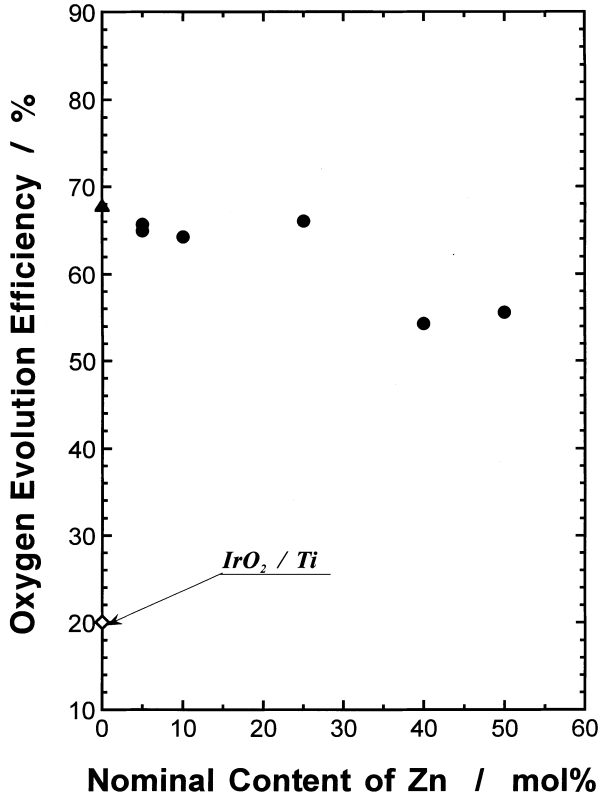

Fig. 4. The oxygen evolution efficiency of as-prepared MnO_X–ZnO/MnO_X/IrO_2/Ti electrodes measured at a current density of 200 A m^{-2} in 0.5 M NaCl at 30 °C and pH 8.3. The efficiency of the IrO_2/Ti electrode is also shown for comparison.

IrO_2/Ti electrode measured in 0.5 M NaCl aqueous solution after leaching of zinc by immersion for different periods of time in the hot alkaline solution. The current density increases with immersion time. As shown in Fig. 1, the surface of the MnO_X–25 mol% ZnO/IrO_2/Ti electrode consists of α-Mn_2O_3 and $ZnMn_2O_4$. Although zinc oxide, ZnO, itself is dissolved almost immediately by immersion in the hot alkaline solution, dissolution of zinc from the spinel type-double oxide $ZnMn_2O_4$ is harder than that of zinc oxide, and hence the current density depends on time of leaching. However, excess immersion, such as more than 6 h, led to the formation of crevices at the interface between the MnO_X layer and the intermediate IrO_2 layer. Accordingly, 6 h was chosen as an adequate immersion time.

Figure 6 shows potentiodynamic anodic polarization curves of MnO_X–ZnO/MnO_X/IrO_2/Ti electrodes after immersion in the hot alkaline solution for 6 h as a function of the nominal zinc content before leaching. The current density increases with the nominal zinc content before leaching. A comparison of Figs 3 and 6 clearly shows that the change in current density with the nominal zinc content is reversed by leaching. It is, therefore, evident that leaching of zinc results in an increase in the effective surface area of the electrode.

Figure 7 shows the oxygen evolution efficiency of surface-activated MnO_X–ZnO/MnO_X/IrO_2/Ti electrodes in electrolysis at 200 A m^{-2} in 0.5 M NaCl at 30 °C as a function of the nominal zinc content before leaching. The efficiency of these electrodes after leaching increases with nominal zinc content up to 25 mol %. The maximum oxygen evolution efficiency of 86% is observed for the surface-activated

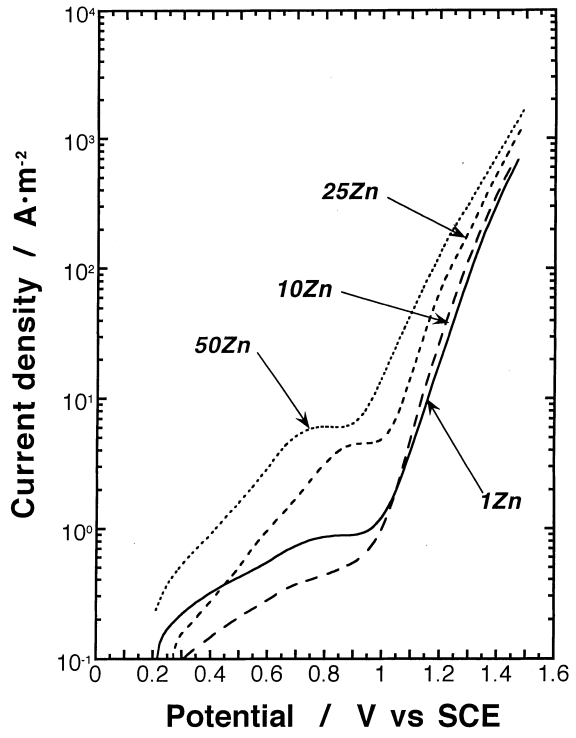

Fig. 6. Potentiodynamic anodic polarization curves of MnO_X–$ZnO/MnO_X/IrO_2/Ti$ electrodes with various initial zinc contents, surface-activated for 6 h, measured in 0.5 M NaCl at 30 °C and pH 8.3–8.7 (Potential IR (ohmic) drop free).

25 mol % zinc electrode. The excess addition of zinc such as 40 mol % decreases the oxygen evolution efficiency in spite of higher current densities than those observed for the electrodes with lower zinc contents.

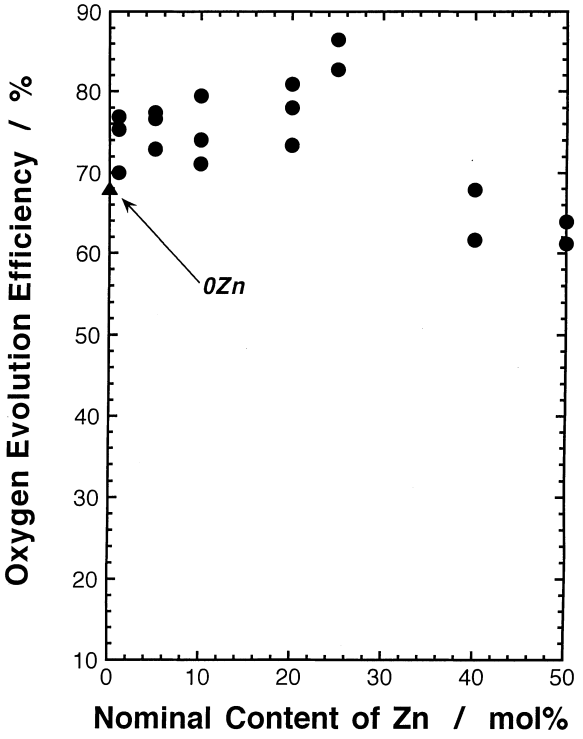

Fig. 7. The oxygen evolution efficiency of surface-activated MnO_X–$ZnO/MnO_X/IrO_2/Ti$ electrodes measured at a current density of 200 A m^{-2} in 0.5 M NaCl at 30 °C and pH 8.3.

For a better understanding of the change in the oxygen evolution efficiency of the surface-activated MnO_X–$ZnO/MnO_X/IrO_2/Ti$ electrodes, X-ray photoelectron spectroscopic analysis was performed. The spectra obtained from the surface of the MnO_X–$ZnO/MnO_X/IrO_2/Ti$ electrodes over a wide binding energy region exhibited peaks of oxygen and carbon in addition to manganese and zinc. The C 1s spectrum arose from a contaminant hydrocarbon layer covering the specimen surface. The O 1s spectrum consisted of a major peak of O^{2-} at about 529.5 eV and a minor shoulder of OH^- and bound water at about 531.3 eV. A peak of the Mn $2p_{3/2}$ spectrum appeared at about 641.4–642.0 eV which is relatively higher than the binding energy of Mn^{2+} $2p_{3/2}$, and the shake-up satellite typical of Mn^{2+} at 5.8–6.0 eV higher than the Mn $2p_{3/2}$ and $2p_{1/2}$ peaks [19–21] was not observed. Accordingly, the Mn $2p_{3/2}$ spectrum is assigned to Mn^{3+} and/or Mn^{4+}. Although Mn^{3+} and Mn^{4+} can be distinguished by the difference in the multiple splitting value of the Mn 3s signal, X-ray diffraction shows that the bulk oxides are composed of α-Mn_2O_3 and $ZnMn_2O_4$ on the electrodes with 25 mol % or less zinc and consist of $ZnMnO_3$ on the electrode with 40 mol % or more zinc, and further distinction of the valence of manganese seems unnecessary for the present objective. No Ir 4f spectrum was observed. The surface composition was determined using integrated intensities of XPS spectra after subtraction of background intensity. Figure 8 shows the cationic fraction of zinc in the surface of the MnO_X–$ZnO/MnO_X/IrO_2/Ti$ electrodes before(○) and after (●) leaching as a function of nominal zinc content before leaching. The cationic fractions of zinc in the surface layer before leaching are even higher than the nominal values. After leaching the cationic fraction of zinc decreases in all electrodes, and

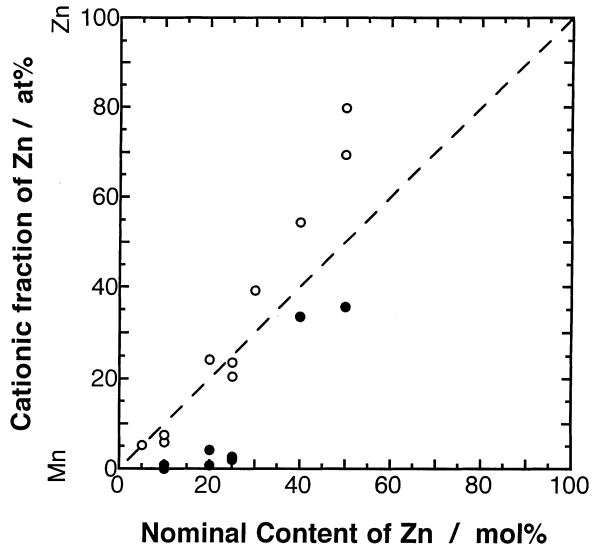

Fig. 8. Cationic fraction of zinc in the surface layer of MnO_X–$ZnO/MnO_X/IrO_2/Ti$ electrodes as a function of the nominal content of zinc in the MnO_X–ZnO layer. Key: (○) as-prepared; (●) surface-activated in 6 M KOH at 80 °C for 6 h.

zinc remaining in the surfaces of electrodes with 1–25 mol % zinc is very small. This indicates that zinc is readily dissolved from $ZnMn_2O_4$. By contrast, dissolution of zinc from the electrodes with 40–50 mol % zinc hardly occurs, because the double oxide $ZnMnO_3$ is barely soluble in the hot alkaline solution.

Figure 9 shows the oxygen evolution efficiency(○) and the cationic fraction of zinc in the electrode surface after leaching(●) as a function of nominal zinc content in the oxide. When the zinc content is adequate, the oxygen evolution efficiency of the MnO_X–$ZnO/MnO_X/IrO_2/Ti$ electrodes after leaching is higher than that of the $MnO_X/IrO_2/Ti$ electrode. In contrast, the addition of excess zinc lowers the efficiency of the MnO_X–$ZnO/MnO_X/IrO_2/Ti$ electrode. Consequently, leaching effectively increases the surface area of the electrodes consisting of 25 mol % or less zinc. In contrast, large amounts of zinc are found undissolved in the electrodes with 40–50 mol % zinc. This indicates that the presence of $ZnMnO_3$ is detrimental to oxygen evolution.

Figure 10 shows scanning electron micrographs of as prepared $MnO_X/IrO_2/Ti$ and MnO_X–25 mol %-$ZnO/MnO_X/IrO_2/Ti$ electrodes, and the MnO_X–25 mol % $ZnO/MnO_X/IrO_2/Ti$ electrode after leaching in hot alkaline solution. As-prepared $MnO_X/IrO_2/Ti$ and MnO_X–25 mol %$ZnO/MnO_X/IrO_2/Ti$ electrode surfaces are fairly smooth. By contrast, the activation by dissolving zinc from the electrode surface is very effective in increasing the effective surface area.

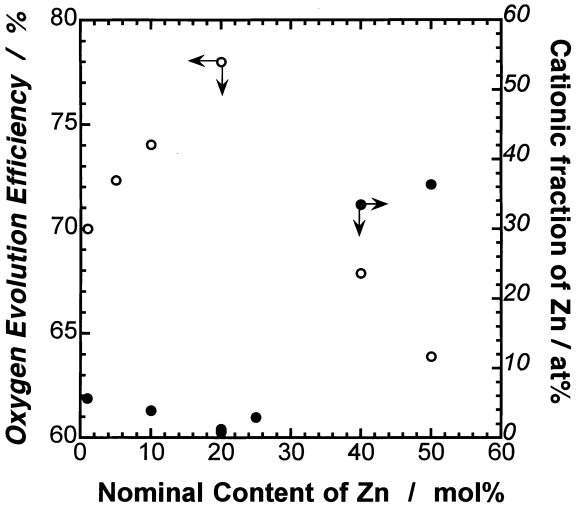

Fig. 9. Oxygen evolution efficiency and cationic fraction of zinc in the surface layer of surface-activated MnO_X–$ZnO/MnO_X/IrO_2/Ti$ electrodes measured at a current density of 200 A m^{-2} in 0.5 M NaCl at 30 °C and pH 8.3 as a function of the nominal zinc content before leaching.

4. Conclusions

An attempt was made to improve the oxygen evolution efficiency of manganese oxide electrode in seawater electrolysis. Manganese oxide was coated on an IrO_2-coated titanium substrate by thermal decomposition. The oxygen evolution efficiency of the $MnO_X/IrO_2/Ti$ electrode is 68–70%.

Since the equilibrium potential of oxygen evolution is lower than that of chlorine evolution, lowering the polarization potential was tried to enhance the oxygen evolution efficiency under the galvanostatic condition by increasing the effective surface area. The increase in the effective surface area was performed by leaching of zinc into hot concentrated KOH from oxide mixtures of manganese and zinc which were coated on the $MnO_X/IrO_2/Ti$ electrode.

Leaching of zinc from the electrodes with 25 mol % or less zinc, whose surface consists of α-Mn_2O_3 and $ZnMn_2O_4$ before leaching, results in significant increase in the oxygen evolution efficiency. The maximum efficiency attained is 86% after leaching of zinc from the MnO_X–25 mol %$ZnO/MnO_X/IrO_2/Ti$ electrode. However, large amounts of zinc addition, such as 40 mol % or more leads to the formation of $ZnMnO_3$, which is hardly dissolved in hot KOH, and

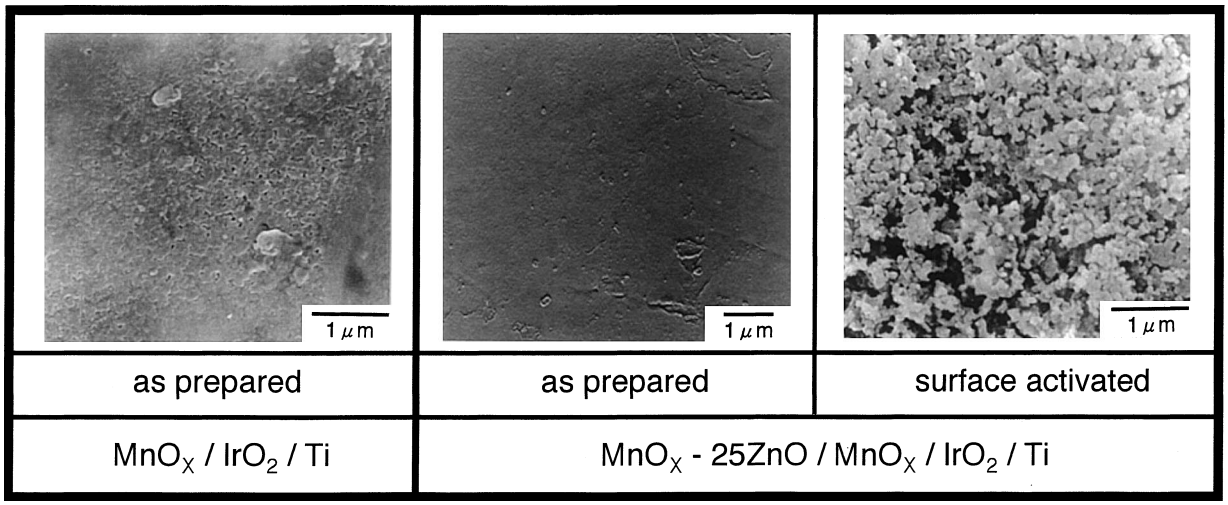

Fig. 10. Scanning electron micrographs of as prepared $MnO_X/IrO_2/Ti$ electrode, as prepared MnO_X–25 mol % $ZnO/MnO_X/IrO_2/Ti$ electrode and MnO_X–25 mol % $ZnO/MnO_X/IrO_2/Ti$ electrode after leaching of zinc in 6 M KOH at 80 °C for 6 h.

gives rise to a decrease in the oxygen evolution efficiency.

Formation of an oxide mixture of manganese and zinc on the electrode surface and subsequent leaching of zinc are effective in enhancing the oxygen evolution efficiency in seawater electrolysis.

Acknowledgements

This work was supported in part by the Grant-in-Aid for Scientific Research (A) no. 07405032 and (A) no. 06402051 from the Ministry of Education, Science and Culture. One of the authors (K.I.) is grateful to the Research Fellowship of the Japan Society for the Promotion of Science for Young Scientists no. 0284.

References

[1] K. Hashimoto, *Mater. Sci. Eng.* **A179**/**A180** (1994) 27.
[2] K. Hashimoto, *Trans. Mater. Res. Soc. Jpn.* **18A** (1994) 35.
[3] K. Hashimoto, E. Akiyama, H. Habazaki, A. Kawashima, K. Shimamura, M. Komori and N. Kumagai, Zairyo-to-Kankyo (*Corrosion Engng*) **45** (1996) 614.
[4] K. Hashimoto, E. Akiyama, H. Habazaki, A. Kawashima, M. Komori, K. Shimamura and N. Kumagai, *Sci. Rep. Res. Inst. Tohoku Univ. A* (1997), in press.
[5] K. Hashimoto, 'Advanced Materials '93, V' (edited by R. Yamamoto, E. Furubayashi, Y. Doi and B. Liu), *Trans. Mater. Res. Soc. Jpn*, Elsevier Science, **18A** (1994) 35.
[6] J. E. Bennet, *Int. J. Hydrogen Energy* **5** (1980) 401.
[7] M. Hiroi, M. Murota, E. Tada and S. Ogawa, *Dennki Kagaku* **57** (1989) 837.
[8] M. Pourbaix, 'Atlas of electrochemical equilibria in aqueous solutions', Pergamon Press (1966).
[9] N. Kumagai, S. Jikihara, Y. Samata, K. Asami and K. Hashimoto, 'Corrosion, electrochemistry and catalysis of metastable metals and intermetallics' (edited by C. R. Clayton and K. Hashimoto), The Electrochemical Society, Pennington, NJ (1994), p. 93.
[10] M. Morita, C. Iwakura and H. Tamura, *Electrochim. Acta* **22** (1977) 325.
[11] A. Kawashima and K. Hashimoto *in* '4th International Conference on Rapidly Quenched Metals', vol. 3 (edited by T. Masumoto and K. Suzuki), Elsevier Science, (1993), p. 1427.
[12] N. Kumagai, Y. Samata, A. Kawashima, K. Asami and K. Hashimoto, *J. Appl. Electrochem.* **3** (1987) 347.
[13] K. Asami, *J. Electron Spectrosc.* **9** (1976) 469.
[14] K. Asami and K. Hashimoto, *Corros. Sci.* **24** (1977) 83.
[15] K. Asami, K. Hashimoto and S. Shimodaira, *ibid.* **17** (1977) 713.
[16] K. Teramoto, K. Asami and K. Hashimoto *ibid.* **27** (1978) 57.
[17] J. H. Scofield, *J. Electron. Spectrosc.* **8** (1976) 129.
[18] M. Morita, C. Iwakura and H. Tamura, *Electrochim. Acta* **23** (1978) 331.
[19] M. Oku, K. Hirokawa and S. Ikeda, *J. Electron Spectrosc.* **7** (1975) 465.
[20] D. Castro and G. Polzonetti, *Chem. Phys. Lett.* **139** (1987) 215.
[21] A. A. El-Moneim, B.-P. Zhang, H. Habazaki, A. Kawashima, K. Asami and K. Hashimoto, *Corros. Sci.* **39** (1997) 305.